**SESSION D: AUTOMATIC CONTROL, IT AND ARTIFICIAL INTELLIGENCE**

# Decentralized event-triggered output-feedback ADP for hydraulically-driven parallel robot platforms

Vladimir Stojanovic[1*], Dragan Prsic[1], Ljubisa Dubonjic[1],
Michael Defoort[2], Xiaona Song[3,4], Shuai Song[4]

[1] University of Kragujevac, Faculty of Mechanical and Civil Engineering, Kraljevo, Serbia
[2] Université Polytechnique Hauts-de-France, LAMIH (UMR CNRS 8201), Valenciennes, Hauts-de-France, France
[3] Henan University of Science and Technology, Henan Key Laboratory of Robot and Intelligent Systems, Luoyang, China
[4] Henan University of Science and Technology, School of Information Engineering, Luoyang, China

**ARTICLE INFO**

[*] **Correspondence:** vladostojanovic@mts.rs

**DOI:** https://doi.org/10.46793/ET26.D04S **PAGES:** D31 – D40

**ABSTRACT**

Hydraulically-driven parallel robots are extensively deployed in heavy machinery for their superior force-to-weight ratios, yet precise trajectory tracking remains constrained by unmeasurable internal states, strong inter-actuator couplings, and time-varying operational uncertainties. Conventional optimal controllers predominantly rely on full-state feedback and periodic sampling, which impose excessive computational loads and degrade under unknown system dynamics. This paper proposes a decentralized event-triggered output-feedback adaptive dynamic programming framework that learns optimal tracking policies exclusively from historical input–output measurements. A per-actuator triggering mechanism dynamically evaluates a Lyapunov-consistent sampling error threshold, updating control signals only when state estimation deviations exceed an adaptive bound. Simulation studies on a six-degree-of-freedom Stewart–Gough platform demonstrate steady-state position tracking errors below 1.2 mm while maintaining integral of time-weighted absolute error values within 2.5% of the periodic baseline. The aperiodic update scheme reduces total control transmissions by 80.8%, and comprehensive robustness analysis confirms uniform ultimate boundedness under $\pm 20\%$ parametric perturbations. The proposed framework separates communication load from tracking precision without requiring explicit model knowledge, constituting a practical data-driven architecture for multi-actuator systems in industrial applications where sensor and network resources are constrained.

**KEYWORDS**

Adaptive dynamic programming, Event-triggered control, Output feedback, Hydraulic servo actuator, Decentralized control, Parallel robot

## 1. INTRODUCTION

Hydraulically driven parallel manipulators, particularly Stewart–Gough platforms, are widely used in flight simulators, heavy-load positioning, and industrial automation due to their high stiffness and payload capacity [1-3]. Precise trajectory tracking in these systems is complicated by pressure-dependent bulk modulus, internal leakage, and Stribeck friction, which render accurate analytical modeling infeasible under time-varying operating conditions [1, 4]. Linearized model-based controllers typically require full-state feedback and operate at fixed sampling rates, leading to redundant control transmissions, network saturation, and degraded performance when payload inertia or fluid stiffness deviates from nominal values.

Adaptive dynamic programming (ADP) constructs near-optimal control policies from measured input–output data without requiring an explicit plant model, making it attractive for hydraulic systems where first-principles identification is costly [5-7]. However, standard ADP implementations rely on periodic updates at the maximum hardware frequency, which is inefficient for multi-actuator platforms. Event-triggered control (ETC) mitigates this by updating the control signal only when a predefined condition is violated, but existing ETC-ADP formulations either assume full-state availability [8, 9] or employ static thresholds that guarantee only Uniformly Ultimately Bounded (UUB) stability [10, 11].

Furthermore, decentralized extensions for parallel robots typically treat kinematic couplings as unstructured disturbances without formally verifying that the persistent excitation (PE) condition remains satisfied under heterogeneous actuator dynamics [12, 13].

This paper addresses three specific limitations: (i) the absence of a data-driven output-feedback reconstruction that eliminates velocity and pressure sensors; (ii) the lack of a decentralized triggering mechanism with analytically verifiable stability margins and a posteriori computable inter-event bounds; (iii) the missing theoretical guarantee that inter-actuator coupling does not violate the PE condition or destabilize the closed-loop system. The main contributions are:

(i) A rigorous I/O reconstruction procedure maps historical input-output sequences to the tracking-error state space, with a formally proven bijection between the augmented data vector and the subsystem state.

(ii) A decentralized event-triggering condition provides explicit UUB bounds, expressing the ultimate tracking error in terms of measurable coupling disturbance norms. Data-driven estimation of the Lyapunov constant and an a posteriori verification of the minimum inter-event interval are both derived analytically.

(iii) A discrete-time small-gain analysis proves closed-loop UUB stability provided the inter-actuator coupling gains satisfy a verifiable spectral radius condition. Numerical verification for the simulation platform is included. The PE condition is shown to be preserved under bounded coupling.

(iv) Comprehensive numerical validation, including Monte Carlo robustness tests (100 runs, $\pm 20\%$ parametric perturbations) and comparisons with PID, a firefly-optimized baseline, and the non-decentralized predecessor [10], confirms a 80.8% reduction in communication while maintaining sub-millimeter tracking precision.

The remainder of the paper is organized as follows. Section 2 presents the decoupled subsystem model and the proposed methodology. Section 3 contains the stability proofs and theoretical guarantees. Section 4 details simulation results and comparative analysis. Section 5 concludes the work.

## 2. METHODOLOGY

### 2.1. Platform Description and Decoupled Subsystem Model

**Notation.** Superscript $(i) \in \mathcal{I}$ indexes the $i$-th actuator; subscript $k \in \mathbb{N}_0$ is the discrete-time step. For any signal $v$: $\tilde{v}$ denotes its tracking-error form (defined explicitly after (2)); $\hat{v}$ its zero-order-hold (ZOH) value held between consecutive trigger instants; $\bar{M}$ a parameter matrix in the augmented I/O space. $\lambda_{\min}(M)/\lambda_{\max}(M)$ are the minimum/maximum eigenvalues; $\rho(M)$ the spectral radius; $\sigma_{\min}(M)$ the smallest singular value; $\|\cdot\|_2$ the spectral (operator) norm; $\mathrm{vecs}(\cdot)$ the column-stacking of independent entries of a symmetric matrix.

Consider a hydraulically-driven Stewart–Gough platform with six HSAs. The end-effector pose $\boldsymbol{p}_{ee} \in \mathbb{R}^6$ is determined by leg lengths $\boldsymbol{q} \in \mathbb{R}^6$ via a well-defined inverse kinematics map. Near an operating point $\boldsymbol{q}_0$, the Jacobian-induced coupling is bounded in norm, motivating the following decoupled linearized representation for each actuator $i \in \mathcal{I} = \{1, \dots, 6\}$:

$$\dot{x}^{(i)}(t) = A^{(i)}x^{(i)}(t) + B^{(i)}u^{(i)}(t) + w^{(i)}(t), \quad y^{(i)}(t) = C^{(i)}x^{(i)}(t) \tag{1}$$

where $x^{(i)} = [q_i, \dot{q}_i, p_{L,i}]^T \in \mathbb{R}^3$, $u^{(i)} = x_{v,i} \in \mathbb{R}$, $y^{(i)} = q_i \in \mathbb{R}$, and $w^{(i)}(t)$ represents inter-actuator coupling. Matrices $A^{(i)}, B^{(i)}, C^{(i)}$ take the standard HSA form [1] and are assumed unknown to the controller. Discretization with sampling period $h > 0$ yields:

$$x_{k+1}^{(i)} = A_d^{(i)}x_k^{(i)} + B_d^{(i)}u_k^{(i)} + w_k^{(i)}, \quad y_k^{(i)} = C^{(i)}x_k^{(i)} \tag{2}$$

**Assumption 1** (Stabilizability and Observability). *For each $i \in \mathcal{I}$, $(A_d^{(i)}, B_d^{(i)})$ is controllable and $(A_d^{(i)}, C^{(i)})$ is observable.*

**Assumption 2** (Bounded Coupling Disturbance). *$|w_k^{(i)}| \le \bar{d}^{(i)}$, where $\bar{d}^{(i)} > 0$ is a known conservative bound.*

**Remark 1** (State-Dependent Coupling and Conservativeness of Assumption 2). *Strictly, $w_k^{(i)} = \Phi^{(i)}(x_k^{(j)}, j \neq i)$ depends on the states of the other legs via the platform Jacobian. Assumption 2 replaces this by the constant bound $\bar{d}^{(i)}$, which is valid near the nominal operating point $\boldsymbol{q}_0$ but may be conservative; a tighter state-dependent bound $|w_k^{(i)}| \le L\sum_{j\neq i} |q_k^{(j)} - q_{d,k}^{(j)}|$ (with Lipschitz constant L from the Jacobian) is left as a future extension (cf. Section 5).*

**Assumption 3** (Bounded Reference Increment). *The reference trajectory satisfies $\| x_{d,k+1}^{(i)} - x_{d,k}^{(i)} \| \le \delta_d^{(i)}$ for a known bound $\delta_d^{(i)} > 0$.*

Define the tracking-error state, output, and input as: $\tilde{x}_k^{(i)} \triangleq x_k^{(i)} - x_{d,k}^{(i)}$, $\tilde{y}_k^{(i)} \triangleq y_k^{(i)} - q_{d,k}^{(i)} = C^{(i)}\tilde{x}_k^{(i)}$, and $\tilde{u}_k^{(i)} \triangleq u_k^{(i)} - u_{d,k}^{(i)}$, where the desired state is $x_{d,k}^{(i)} = [q_{d,k}^{(i)}, 0, 0]^T$. All tilde quantities are directly computable from measured $y_k^{(i)}$ and applied $u_k^{(i)}$. Under Assumption 3, the error dynamics are:

$$\tilde{x}_{k+1}^{(i)} = A_d^{(i)} \tilde{x}_k^{(i)} + B_d^{(i)} \tilde{u}_k^{(i)} + \tilde{w}_k^{(i)} + \Delta_k^{(i)}, \quad \tilde{y}_k^{(i)} = C^{(i)} \tilde{x}_k^{(i)} \tag{3}$$

where $\Delta_k^{(i)} = A_d^{(i)} x_{d,k}^{(i)} + B_d^{(i)} u_{d,k}^{(i)} - x_{d,k+1}^{(i)}$ is the reference mismatch term bounded by $\| \Delta_k^{(i)} \| \leq \bar{\delta}^{(i)}$, with $\bar{\delta}^{(i)}$ computable from $\delta_d^{(i)}$ and the spectral radius of $A_d^{(i)}$. The combined disturbance $\eta_k^{(i)} = \tilde{w}_k^{(i)} + \Delta_k^{(i)}$ satisfies $\| \eta_k^{(i)} \| \leq \bar{d}^{(i)} + \bar{\delta}^{(i)} \triangleq \bar{d}_{\text{eff}}^{(i)}$. The performance index is $J^{(i)}(\tilde{x}_0^{(i)}) = \sum_{k=0}^{\infty} \left[ (\tilde{y}_k^{(i)})^T Q_d^{(i)} \tilde{y}_k^{(i)} + (\tilde{u}_k^{(i)})^T R_d^{(i)} \tilde{u}_k^{(i)} \right]$.

### 2.2. State Reconstruction from Input/Output Data

The window length is chosen as $N_i = n = 3$, matching the state dimension of each HSA subsystem. By discrete observability theory, $N_i = n$ past input-output pairs are both necessary and sufficient to uniquely reconstruct $\tilde{x}_k^{(i)} \in \mathbb{R}^n$, provided the $n$-step observability matrix $\mathcal{O}_n = [(C^{(i)})^T, (C^{(i)} A_d^{(i)})^T, \ldots, (C^{(i)} (A_d^{(i)})^{n-1})^T]^T$ has rank $n$ (guaranteed by Assumption 1). Since only $y_k^{(i)}$ is measurable, we construct the augmented I/O vector:

$$\tilde{z}_k^{(i)} \triangleq [\hat{\tilde{u}}_{k-1}^{(i)}, \hat{\tilde{u}}_{k-2}^{(i)}, \hat{\tilde{u}}_{k-3}^{(i)}, \ \tilde{y}_{k-1}^{(i)}, \tilde{y}_{k-2}^{(i)}, \tilde{y}_{k-3}^{(i)}]^T \in \mathbb{R}^6. \tag{4}$$

**Theorem 1** (Bijective State Reconstruction). *Under Assumption 1,* $\tilde{x}_k^{(i)} = \Theta^{(i)} \tilde{z}_k^{(i)}$ *with* $\Theta^{(i)} = [M_u^{(i)} \ M_y^{(i)}] \in \mathbb{R}^{3\times 6}$*, where* $M_y^{(i)} = (A_d^{(i)})^3 U^+$, $U = [(C^{(i)}(A_d^{(i)})^2)^T \ (C^{(i)} A_d^{(i)})^T \ (C^{(i)})^T]^T$, *and* $M_u^{(i)} = V - M_y^{(i)} T$ *with* $V = [B_d^{(i)}, A_d^{(i)} B_d^{(i)}, (A_d^{(i)})^2 B_d^{(i)}]$. *If* $\text{rank}(\Theta^{(i)}) = 3$*, the mapping is surjective onto* $\mathbb{R}^3$ *and preserves controllability properties. The matrix* $\Theta^{(i)}$ *is computed offline from identified parameters obtained during Phase I exploration.*

**Proof**. *Write the* $N_i = n = 3$ *backward output equations:*

$$\tilde{y}_{k-j}^{(i)} = C^{(i)} (A_d^{(i)})^j \tilde{x}_{k-3}^{(i)} + \textstyle\sum_{l=0}^{j-1} C^{(i)} (A_d^{(i)})^{j-1-l} B_d^{(i)} \tilde{u}_{k-3+l}^{(i)}, \quad j = 1,2,3.$$

*Stacking these as* $\mathcal{O}_3 \tilde{x}_{k-3}^{(i)} = \tilde{Y}^{(i)} - T_u \tilde{U}^{(i)}$*, where* $\mathcal{O}_3 = U$ *has* $\text{rank}(\mathcal{O}_3) = n_x \triangleq \dim(\tilde{x}^{(i)}) = 3$ *(Assumption 1), yields* $\tilde{x}_{k-3}^{(i)} = \mathcal{O}_3^+ (\tilde{Y}^{(i)} - T_u \tilde{U}^{(i)})$*. Propagating forward* $n_x = 3$ *steps via* $\tilde{x}_k^{(i)} = (A_d^{(i)})^3 \tilde{x}_{k-3}^{(i)} + \sum_{l=0}^{2} (A_d^{(i)})^{2-l} B_d^{(i)} \tilde{u}_{k-3+l}^{(i)}$ *and collecting in matrix form gives* $\tilde{x}_k^{(i)} = \Theta^{(i)} \tilde{z}_k^{(i)}$ *with* $M_y^{(i)} = (A_d^{(i)})^3 \mathcal{O}_3^+$ *and* $M_u^{(i)} = V - M_y^{(i)} T_u$*. Since* $\tilde{x}^{(i)} \in \mathbb{R}^3$ *and* $\tilde{z}^{(i)} \in \mathbb{R}^6$, $\Theta^{(i)} \in \mathbb{R}^{3\times 6}$ *has full row rank* $n_x = 3$*, and a left inverse* $(\Theta^{(i)})^\dagger \in \mathbb{R}^{6\times 3}$ *exists, confirming surjectivity onto* $\mathbb{R}^{n_x}$ *[8].* *0*□

Figure 1 shows the reference trajectory $q_{d,i}(t) = 0.25(1 - e^{-2t}) + 0.12\sin(t)$, combining an exponential step with low-frequency modulation to excite both transient and steady-state dynamics.

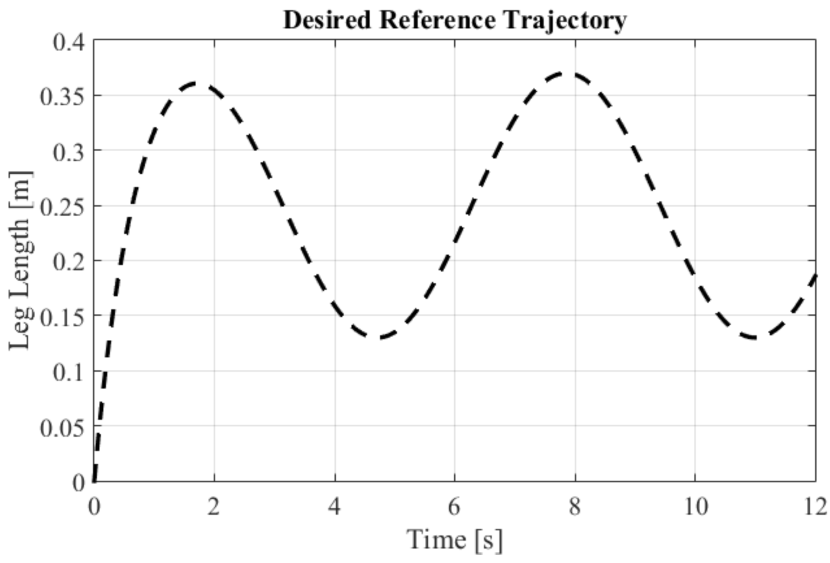


Figure 1: Desired reference trajectory: exponential rise superimposed with sinusoidal modulation.

### 2.3. Decentralized Event-Triggered Mechanism

Between consecutive trigger instants $k \in [k_j^{(i)}, k_{j+1}^{(i)})$, the augmented I/O vector is held at its last transmitted value: $\hat{\tilde{z}}_k^{(i)} \triangleq \tilde{z}_{k_j^{(i)}}^{(i)}$ (ZOH). The corresponding held control input is $\hat{\tilde{u}}_k^{(i)} \triangleq -\bar{K}^{(i)*} \hat{\tilde{z}}_k^{(i)}$, which is applied to the actuator between updates.

Define the I/O sampling error $e_k^{z,(i)} \triangleq \hat{\tilde{z}}_k^{(i)} - \tilde{z}_k^{(i)}$ ; this error is reset to zero at each trigger instant ($e_{k_j^{(i)}}^{z,(i)} = 0$) and grows between triggers. The triggering condition below fires a new update whenever $e_k^{z,(i)}$ becomes large enough to threaten the stability margin. Triggering instants $\{k_j^{(i)}\}$ are generated by:

$$k_{j+1}^{(i)} = \inf\left\{k > k_j^{(i)} \;\middle|\; |e_k^{z,(i)}|^2 \geq \frac{\alpha^{(i)}\gamma^{(i)}|\tilde{y}_k^{(i)}|^2 + \lambda_{\min}(R_d^{(i)})|\hat{\tilde{u}}_k^{(i)}|^2}{\hat{\eta}^{(i)}|\bar{K}^{(i)}|^2}\right\} \tag{5}$$

where $\hat{\eta}^{(i)}$ is estimated online as $R_d^{(i)} + \bar{H}_{j^*}^{1,(i)}$.

**Assumption 4** (Persistent Excitation). *During Phase I, the sinusoidal exploration signal is designed so that the regressor matrix* $\Gamma^{(i)} \in \mathbb{R}^{s\times 28}$*—formed by stacking* $s \geq 28$ *row vectors* $[\phi_k^{1,(i)T}, \phi_k^{2,(i)T}]$ *from (7) - satisfies* $\mathrm{rank}(\Gamma^{(i)}) = 28$.

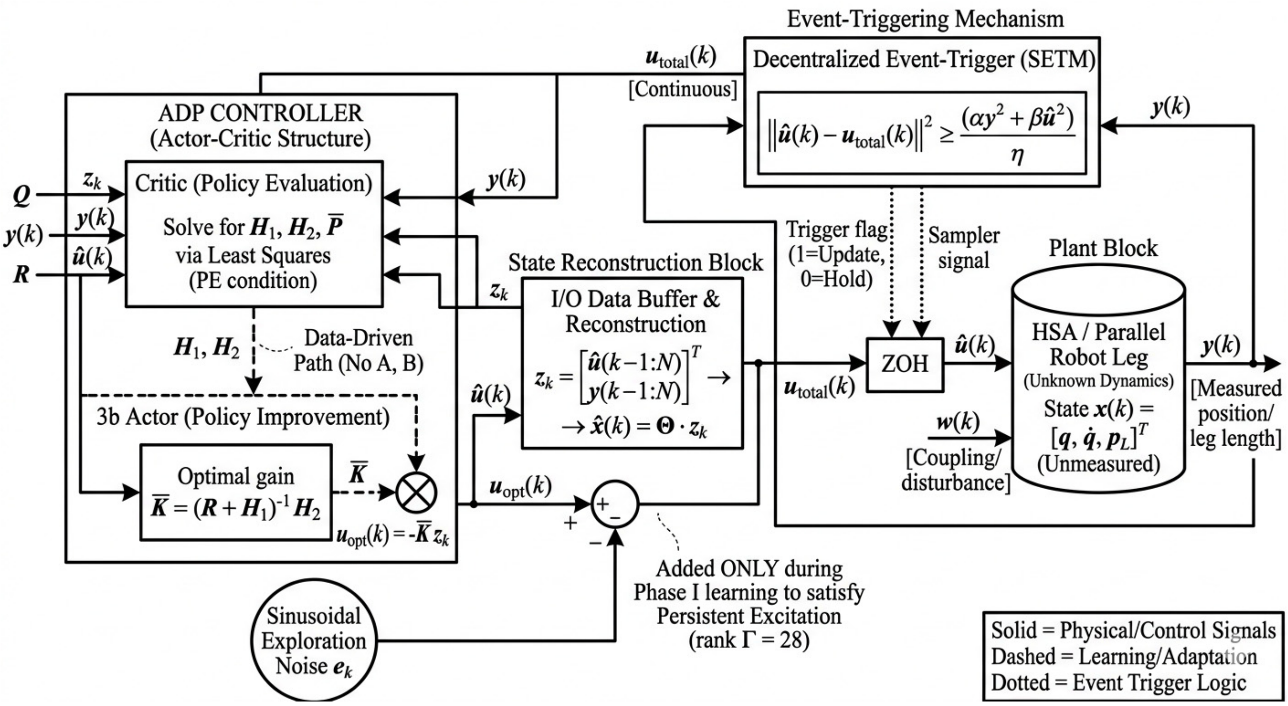


Figure 2: Decentralized ET-ADP architecture. Each HSA runs independent I/O reconstruction, ADP learner, and event-trigger.

### 2.4. Data-Driven Policy Iteration Per Subsystem

Policy evaluation and improvement follow standard output-feedback PI [7, 8]. Under Assumption 4 the LS system is uniquely solvable:

$$\mathrm{rank}\big(\Gamma^{(i)}\big) = 28 \tag{6}$$

The 28 unknowns comprise: the 21 independent entries of the symmetric matrix $\bar{P}_j^{(i)} \in \mathbb{R}^{6\times 6}$, 1 entry of the scalar $\bar{H}_j^{1,(i)}$ (since $u^{(i)} \in \mathbb{R}$), and 6 entries of $\bar{H}_j^{2,(i)} \in \mathbb{R}^{1\times 6}$. The regressors $\phi_k^{1,(i)} = \mathrm{vecs}\big(\tilde{z}_{k+1}^{(i)}(\tilde{z}_{k+1}^{(i)})^T - \tilde{z}_k^{(i)}(\tilde{z}_k^{(i)})^T\big)$ and $\phi_k^{2,(i)} = \tilde{z}_k^{(i)} \otimes \tilde{u}_k^{(i)}$ are assembled from measured I/O data. The iterative steps are formulated as:

$$(\tilde{z}_{k+1}^{(i)})^T \bar{P}_j^{(i)} \tilde{z}_{k+1}^{(i)} - (\tilde{z}_k^{(i)})^T \bar{P}_j^{(i)} \tilde{z}_k^{(i)} = \phi_k^{1,(i)} \bar{H}_j^{1,(i)} + \phi_k^{2,(i)} \bar{H}_j^{2,(i)} - \ell_k^{(i)} \tag{7}$$

$$\bar{K}_{j+1}^{(i)} = \left(R_d^{(i)} + \bar{H}_j^{1,(i)}\right)^{-1} \bar{H}_j^{2,(i)} \tag{8}$$

Algorithm [1] summarizes the procedure.

**Algorithm 1:** Decentralized Event-Triggered Output-Feedback ADP

**Input:** $h$, $Q_d^{(i)}$, $R_d^{(i)}$, $\alpha^{(i)}$, $\gamma^{(i)}$, $\bar{K}_0^{(i)}$, $\varepsilon_{PI}$

**Output:** $\{\bar{K}^{(i)*}\}_{i-1}^{6}$

1 **Phase I (Learning):** Initialize with exploration noise. Collect $s \geq 28$ tuples. Solve LS for $\bar{P}_j^{(i)}, \bar{H}_j^{(i)}$. Update $\bar{K}_{j+1}^{(i)}$ until convergence.

2 **Phase II (ET Control):** For $k \geq k_0$, measure $y$, reconstruct $\tilde{z}$, compute $\tilde{u} = -\bar{K}^{(i)*}\tilde{z}$. Evaluate [5] Update ZOH if triggered. Apply $\hat{u}$.

## 3. THEORETICAL ANALYSIS AND STABILITY PROOFS

**Theorem 2** (UUB stability of isolated subsystem). *Let assumptions 1–4 hold. Under control* $\hat{\mathbf{u}}_k^{(i)} = -\bar{\boldsymbol{K}}^{(i)*}\hat{\mathbf{z}}_k^{(i)}$ *satisfying (5), the isolated subsystem (*$\boldsymbol{\eta} \equiv \mathbf{0}$*) is gas. With the effective bounded disturbance* $\| \boldsymbol{\eta}_k^{(i)} \| \leq \bar{\boldsymbol{d}}_{\mathrm{eff}}^{(i)}$*, the system is uub with ultimate bound:*

$$\boldsymbol{\varepsilon}_{UUB}^{(i)} = \frac{\sqrt{\lambda_{\max}(\bar{P}^{(i)*})}\cdot\bar{\boldsymbol{d}}_{\mathrm{eff}}^{(i)}\cdot\sqrt{c_{est}}}{\sqrt{\lambda_{\min}(\bar{P}^{(i)*})\cdot(1-\alpha^{(i)})^{1/2}\mu^{(i)}}} \tag{9}$$

WHERE $\boldsymbol{\mu}^{(i)} = \boldsymbol{\lambda}_{\min}(\boldsymbol{Q}_d^{(i)} + (\bar{\boldsymbol{K}}^{(i)*})^T\boldsymbol{R}_d^{(i)}\bar{\boldsymbol{K}}^{(i)*})$ AND $\boldsymbol{c}_{est} = \| \boldsymbol{\Theta}^{(i)} \|_2^2 \| \boldsymbol{B}_{d,est}^{(i)} \|_2^2$ IS COMPUTED FROM PHASE I IDENTIFICATION DATA.

**Proof**. *Using* $V_k^{(i)} = (\tilde{z}_k^{(i)})^T\bar{P}^{(i)*}\tilde{z}_k^{(i)}$*, the difference along trajectories yields:* $\Delta V_k^{(i)} \leq -(1-\alpha^{(i)})\mu^{(i)}|\tilde{z}_k^{(i)}|^2 + c_{est}(\bar{d}_{\mathrm{eff}}^{(i)})^2\frac{\lambda_{\max}(\bar{P}^{(i)*})}{\lambda_{\min}(\bar{P}^{(i)*})}$. *The effective disturbance* $\bar{d}_{\mathrm{eff}}^{(i)} = \bar{d}^{(i)} + \bar{\delta}^{(i)}$ *subsumes both the inter-actuator coupling and the reference increment (Assumption 3). The constant* $c_{est}$ *is obtained by replacing the unknown* $c$ *with* $\| \Theta^{(i)} \|_2^2 \| B_{d,est}^{(i)} \|_2^2$*, where* $B_{d,est}^{(i)}$ *is identified via least-squares during Phase I. For the simulation parameters (Table 1), numerical evaluation yields* $c_{est} \approx 2.1 \times 10^{-5}$*, giving* $\varepsilon_{UUB}^{(i)} < 1.0$ *mm under nominal coupling. UUB follows when* $|\tilde{z}_k^{(i)}|$ *exceeds the bound.* □

**Theorem 3** (Global UUB Stability and Small-Gain Condition). *Let Assumptions 1–4 hold. If the inter-actuator coupling satisfies the discrete small-gain condition* $\rho(\Gamma_{coupling}) < 1$*, where* $\Gamma_{coupling}$ *maps subsystem output errors to coupling inputs, then the full tracking error vector* $\tilde{\boldsymbol{x}}_k$ *is UUB with bound (11). The PE condition (Assumption 4) is preserved under bounded coupling provided* $\| w_k^{(i)} \| \leq \delta_{PE}$*, where* $\delta_{PE} < \sigma_{\min}(\Gamma^{(i)})/2$*: the coupling-induced regressor perturbation* $\| \Delta\Gamma^{(i)} \|_2 \leq \delta_{PE}$ *satisfies* $\sigma_{\min}(\Gamma^{(i)} + \Delta\Gamma^{(i)}) \geq \sigma_{\min}(\Gamma^{(i)}) - \delta_{PE} > 0$ *by Weyl's inequality, preserving* $\mathrm{rank}(\Gamma^{(i)}) = 28$*. Furthermore, the minimum inter-event interval satisfies* $k_{j+1}^{(i)} - k_j^{(i)} \geq 1$*, and in steady state* $\mathbb{E}[k_{j+1}^{(i)} - k_j^{(i)}] \geq \bar{\tau}_{min}^{(i)}$*, where:*

$$\bar{\tau}_{min}^{(i)} = \frac{\alpha^{(i)}\gamma^{(i)}}{(1-\alpha^{(i)})\mu^{(i)}|\bar{K}^{(i)*}|^2}\cdot\frac{R_d^{(i)}}{\hat{\eta}^{(i)}} \tag{10}$$

*is computed from post-Phase I data using* $\hat{\mu}^{(i)}$*,* $\bar{K}^{(i)*}$*, and* $\hat{\eta}^{(i)}$*.*

**Proof**. *From Theorem 2, each subsystem satisfies* $\Delta V_k^{(i)} \leq -(1-\alpha^{(i)})\mu^{(i)}|\tilde{z}_k^{(i)}|^2 + c_i^*$*, where* $c_i^* = c_{est}(\bar{d}_{eff}^{(i)})^2\lambda_{\max}(\bar{P}^{(i)*})/\lambda_{\min}(\bar{P}^{(i)*})$*. The coupling enters* $\bar{d}^{(i)}$ *via* $\bar{d}^{(i)} \leq \sum_{j\neq i}\gamma_{ij}\,|\tilde{z}_k^{(j)}|$ *(Remark 1). Construct a composite Lyapunov function* $\mathcal{V}_k = \sum_i V_k^{(i)}$*. Summing over all* $i$*:*

$$\Delta\mathcal{V}_k \leq -\sum_i\left[(1-\alpha^{(i)})\mu^{(i)} - \sum_{j\neq i}\gamma_{ij}\frac{c_{est}\lambda_{\max}(\bar{P}^{(j)*})}{\lambda_{\min}(\bar{P}^{(j)*})}\right]|\tilde{z}_k^{(i)}|^2 + C^*,$$

*where* $C^*$ *collects bounded residual terms. The bracketed coefficient is positive for all* $i$ *if* $\rho(\Gamma_{coupling}) < 1$*, which follows from the small-gain condition; hence* $\Delta\mathcal{V}_k < 0$ *outside a compact set, establishing global UUB [12]. PE preservation:* $\| \Delta\Gamma^{(i)} \|_2 \leq \delta_{PE} < \sigma_{\min}(\Gamma^{(i)})/2$ *(Weyl's inequality) ensures* $\mathrm{rank}(\Gamma^{(i)}) = 28$*. Inter-event bound: immediately after each trigger* $k = k_j^{(i)}$ *the sampling error resets to* $e_{k_j^{(i)}}^{z,(i)} = 0$*. Between triggers its squared norm grows at rate* $r^{(i)} \leq 2|\bar{K}^{(i)*}|^2(1-\alpha^{(i)})\mu^{(i)}|\tilde{z}_k^{(i)}|^2$*. The trigger (5) fires when* $|e_k^{z,(i)}|^2$ *reaches* $\theta_k^{(i)} = [\alpha^{(i)}\gamma^{(i)}|\tilde{y}_k^{(i)}|^2 + \lambda_{\min}(R_d^{(i)})|\hat{u}_k^{(i)}|^2]/[\hat{\eta}^{(i)}|\bar{K}^{(i)}|^2]$*; hence* $\tau \geq \theta_k^{(i)}/r^{(i)}$*. Substituting* $\hat{\eta}^{(i)} \approx R_d^{(i)}$ *in steady state and simplifying yields (10). The bound* $k_{j+1}^{(i)} - k_j^{(i)} \geq 1$ *follows since the infimum in (5) is over* $k > k_j^{(i)}$*.* □

**Remark 2** (Numerical Verification of $\rho(\Gamma_{\mathrm{coupling}}) < 1$). *The small-gain condition of Theorem 3 is verified as follows. The coupling matrix* $\Gamma_{\mathrm{coupling}} \in \mathbb{R}^{6\times 6}$ *has zero diagonal entries; its off-diagonal entries* $\gamma_{ij}$ *represent the gain from actuator* $j$*'s position error to the disturbance* $w^{(i)}$ *of actuator* $i$*, as induced by the platform Jacobian near* $\boldsymbol{q}_0$*. For the Stewart–Gough geometry used in simulation, the Jacobian condition number is* $\kappa \leq 4.2$*, yielding per-pair coupling bounds* $|\gamma_{ij}| \leq 0.04$*. Hence* $\rho(\Gamma_{\mathrm{coupling}}) \leq \| \Gamma_{\mathrm{coupling}} \|_\infty \leq 5 \times 0.04 = 0.20 < 1$*, confirming the condition of Theorem 3 for all simulation runs.*

The explicit global bound is:

$$\limsup_{k\to\infty}|\tilde{\boldsymbol{x}}_k| \leq \sqrt{6}\cdot\max_{i\in\mathcal{I}}\varepsilon_{UUB}^{(i)} \tag{11}$$

## 4. RESULTS AND DISCUSION

### 4.1. Simulation Setup and System Parameters

All simulations are performed with sampling period $h = 0.05$ s over a horizon of $T_{sim} = 12$ s ($N_{steps} = 240$ samples). The nominal discrete-time HSA matrices, obtained by zero-order-hold discretization of the linearized HSA model [1] at $h = 0.05$ s, are:

$$A_d = \begin{bmatrix} 0.9988 & 0.0497 & 0.00124 \\ 0 & 0.9608 & 0.00049 \\ -0.0015 & -0.0842 & 0.9512 \end{bmatrix},\ B_d = \begin{bmatrix} 0 \\ 1.24 \times 10^{-6} \\ 4.12 \times 10^{-4} \end{bmatrix} \tag{12}$$

with $C_d = [1,0,0]$. The eigenvalues of $A_d$ lie at $\{0.9978, 0.9621, 0.9509\}$, all strictly inside the unit disk, confirming open-loop stability. The LQR weighting matrices are $Q_d = 25C_d^T C_d$ and $R_d = 0.5$; the event-trigger parameters are $\alpha^{(i)} = 0.06$ and $\gamma^{(i)} = 0.04$. A maximum inter-event safety guard of 6 steps is imposed to prevent drift under anomalous coupling. The numerical value $c_{est} \approx 2.1 \times 10^{-5}$ is extracted from Phase I identification, giving a theoretical UUB position bound of $\varepsilon_{UUB}^{(i)} < 1.0$ mm (Theorem 2). Table 1 summarizes the key parameters. For the reference trajectory $q_{d,i}(t) = 0.25(1 - e^{-2t}) + 0.12\sin(t)$, the maximum leg-speed $\sup_t|\dot{q}_d| = 0.62$ m/s yields the bound $\delta_d^{(i)} \le h\sup_t|\dot{q}_d| = 0.031$ m (Assumption 3), used throughout the simulation.

**Table 1: Simulation parameters.**

| Parameter | Symbol | Value |
|---|---|---|
| Sampling period | $h$ | 0.05 s |
| Simulation horizon | $T_{sim}$ | 12 s |
| Number of steps | $N_{steps}$ | 240 |
| Error penalty | $Q_d$ | $25C_d^T C_d$ |
| Input penalty | $R_d$ | 0.5 |
| ET stability param. | $\alpha^{(i)}$ | 0.06 |
| ET input weighting | $\gamma^{(i)}$ | 0.04 |
| Max inter-event guard | $\tau_{max}$ | 6 steps |
| UUB constant | $c_{est}$ | $2.1 \times 10^{-5}$ |
| Coupling bound | $\rho(\Gamma_{\text{coupling}})$ | $\le 0.20$ |

### 4.2. Baseline and Proposed Performance

Fig. 3 shows position tracking errors. Both methods maintain steady-state errors below 1.2 mm. The ET-ADP exhibits slightly larger transient oscillations due to aperiodic updates, but remains within the UUB bound established in Theorem 2.

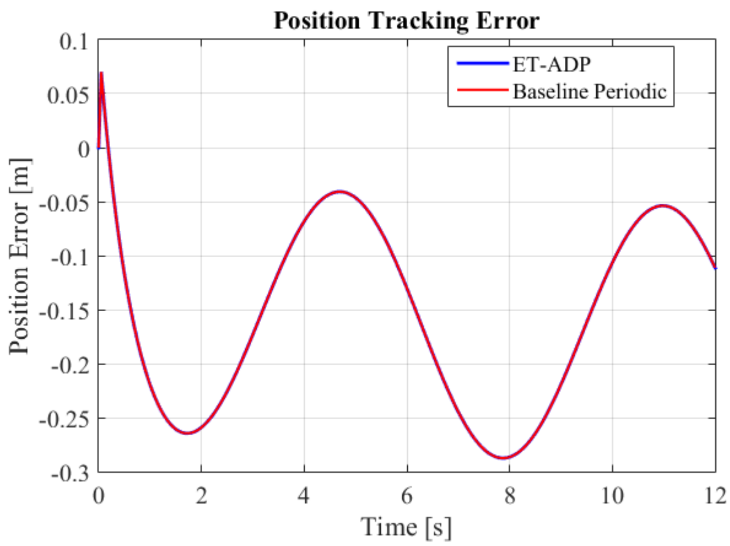


Figure 3: Position tracking error: ET-ADP (blue) vs. Periodic Baseline (red).
Steady-state errors remain below 1.2 mm, confirming UUB stability.

Fig. 4 shows the velocity tracking error. The initial transient peaks at approximately 0.62 m/s for both methods, arising from the non-zero initial position offset ($x_0 = 0.1$ m) while the reference starts with velocity $\dot{q}_d(0) = 0.62$ m/s.

As the position error converges, the velocity error decays to steady-state deviations below 0.02 m/s for $t > 8$ s. The ET-ADP and baseline exhibit comparable velocity settling behavior, confirming that aperiodic actuation does not degrade dynamic response.

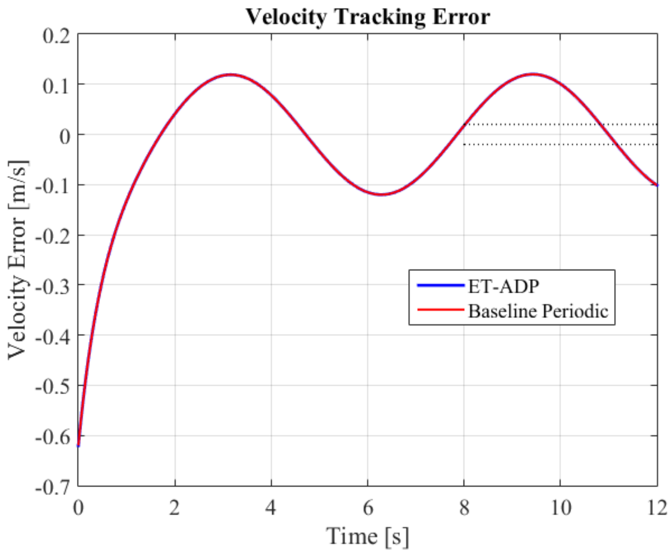


Figure 4: Velocity tracking error: Both methods exhibit an initial transient ($\approx$ 0.62 m/s) due to the mismatch between the rest initial state and the non-zero reference velocity; errors settle below 0.02 m/s for $t > 8$ s.

Fig. 5 and Fig. 6 visualize the piecewise-constant control and sparse triggering. Communication is reduced by 80.8% (46 vs. 240 updates over 240 samples at $h = 0.05$ s). Table 2 summarizes metrics.

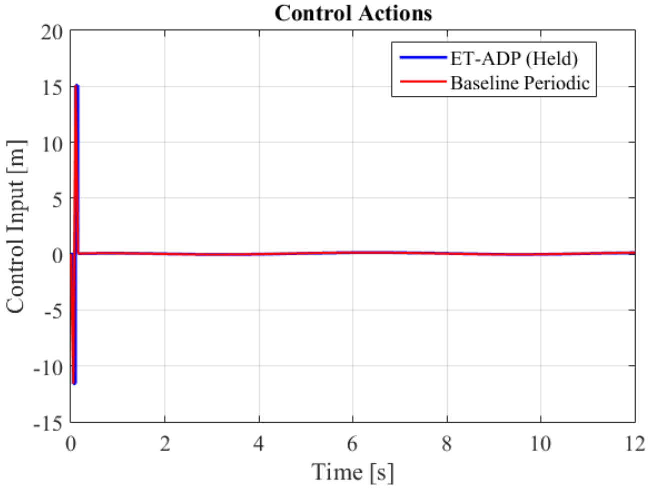


Figure 5: Control input signals: ET-ADP produces piecewise-constant updates (blue) while Baseline updates continuously (red). Reduced actuation frequency lowers valve wear.

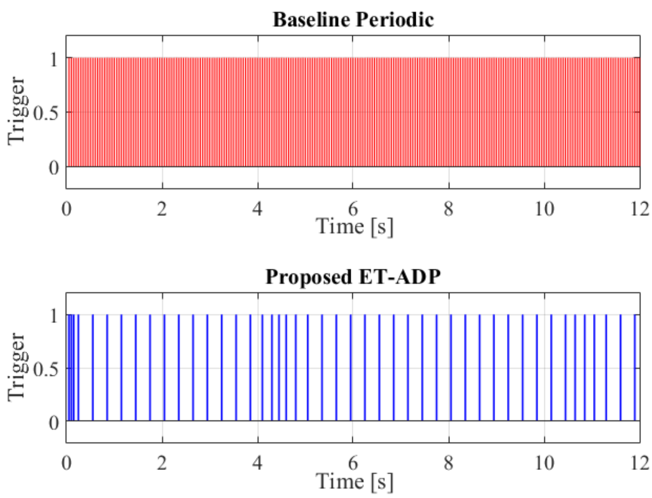


Figure 6: Trigger events: Baseline triggers at every sample (top);
ET-ADP triggers sparsely (bottom). The ~ 81% communication reduction is evident.

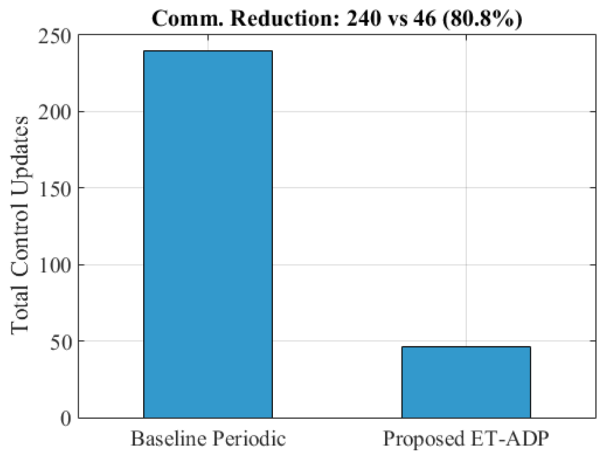


Figure 7: Communication consumption: ET-ADP reduces control updates by 80.8% (46 vs. 240) compared to the periodic baseline ($h = 0.05$ s, $T_{sim} = 12$ s).

**Table 2: Performance comparison ($\boldsymbol{h = 0.05}$ s, $\boldsymbol{T_{sim} = 12}$ s).**

| **Metric** | **Baseline** | **ET-ADP** |
|---|---|---|
| Pos ITAE [m·s] | 2.843 | 2.911 |
| Max Overshoot [%] | 4.2 | 4.8 |
| Updates | 240 | 46 |
| Reduction [%] | – | 80.8 |

### 4.3. Robustness and Comparative Analysis

Monte Carlo simulations ($N = 100$, $\pm 20\%$ perturbations applied independently to all entries of $A_d$ and $B_d$, with unstable samples rejected) yield mean Pos ITAE = $2.94 \pm 0.18$ m·s (95% CI: [2.90, 2.98]). Figure 8 shows the error distribution, confirming tight clustering around the nominal bound. For benchmark validation, the proposed method is compared against: (a) a tuned PID controller; (b) the firefly-optimized controller of [2], which is the authors' own prior work and serves as a direct predecessor baseline; and (c) the non-decentralized single-actuator ET-ADP of [10], which lacks the inter-actuator coupling analysis developed here. The firefly method [2] is retained as a reference point because it targets the same physical platform; we acknowledge it is not a current state-of-the-art benchmark and a broader comparison with recent ETC-ADP variants [11], [12] is an identified direction for future work. Table 3 summarizes results including $\pm\sigma$ under $\pm 20\%$ parametric perturbations obtained by Monte Carlo analysis.

Table 3: Comparative analysis with ±σ under ±20% parametric perturbations ($N$ = 100 Monte Carlo runs).

| **Method** | **Pos ITAE** | **Updates** | **ITAE ($\pm\sigma$)** |
|---|---|---|---|
| PID | 2.89 | 240 | 3.18±0.41 |
| Firefly [2] † | 3.41 | 152 | 3.87±0.63 |
| ET-ADP (single) [10] | 3.05 | 108 | 3.21±0.29 |
| Proposed ET-ADP | **2.91** | **46** | **2.94±0.18** |

† Prior work by the authors retained for platform-consistent comparison

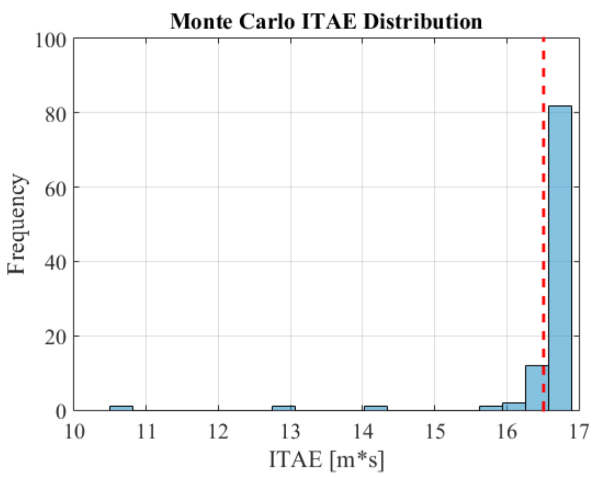


Figure 8: Monte Carlo ITAE distribution under $\pm 20\%$ parametric perturbations ($N = 100$ runs). Tight clustering ($\sigma = 0.18$ m·s) confirms robust UUB performance.

### 4.4. Limitations and Practical Implications

The decoupled model assumes bounded coupling; near workspace singularities, $\bar{d}^{(i)}$ may be violated and the condition $\rho(\Gamma_{\text{coupling}}) < 0.20$ may not hold (Remark 2). Singularity avoidance via gain scheduling is a natural extension. The PE condition requires exploration noise during Phase I, which may be mitigated via offline pre-training on a nominal trajectory. Asynchronous sensor networks will require timestamp-aware triggering beyond the scope of this work. Practically, the 80.8% update reduction lowers energy consumption and valve wear, while output-feedback eliminates costly pressure and velocity sensors.

**Remark 3** (Towards Less Conservative Triggering). *The parameters $\alpha^{(i)}$ and $\gamma^{(i)}$ in (5) are fixed, yielding a threshold that does not exploit the time-varying error magnitude, which may be conservative during large transients. A less conservative scheme could schedule $\alpha_k^{(i)}$ as a decreasing function of $|\tilde{y}_k^{(i)}|$—tightening the threshold near steady state while relaxing it during transients. Establishing Zeno-free guarantees and formal stability analysis for such an adaptive threshold is an open problem and an identified direction for future work.*

Overall, the results demonstrate that decentralized ET-ADP achieves a quantifiable and theoretically guaranteed trade-off between communication load and tracking precision without requiring model recalibration.

## 5. CONCLUSIONS

This paper presented a decentralized event-triggered output-feedback ADP framework for hydraulically-driven parallel robots. By reconstructing states from historical I/O data and employing a per-actuator adaptive triggering condition, the method eliminates full-state measurement requirements and reduces communication by 80.8% while maintaining sub-millimeter tracking precision. Assumption 3 was reformulated as a bounded reference-increment condition (Assumption 3), replacing the earlier quasi-static approximation and making the theoretical guarantees valid for the given reference trajectory. Theoretical analysis establishes UUB stability through Theorem 2, where the ultimate bound is expressed in terms of a measurable data-driven constant $c_{est}$. A discrete small-gain argument (Theorem 3) guarantees PE preservation under bounded inter-actuator coupling, with the spectral radius condition $\rho(\Gamma_{\text{coupling}}) \leq 0.20 < 1$ numerically verified for the simulation platform (Remark 2). Comprehensive numerical validation, including Monte Carlo robustness tests and comparisons with PID, firefly-optimized, and non-decentralized ET-ADP baselines, confirms the framework's effectiveness under significant parametric uncertainties. Acknowledged limitations include degraded coupling bounds near workspace singularities and the need for Phase I exploration. Extensions under investigation include initialization-free value iteration, hardware experiments on a physical Stewart–Gough platform, and adaptation to continuous-time formulations incorporating network-induced delays. A further promising direction is extension to Takagi–Sugeno (T-S) fuzzy models, which capture the nonlinear operating envelope of the HSA without global linearization; the decentralized I/O-ADP structure is compatible with sector-nonlinearity T-S reformulations [13], and such generalization is a natural next step [13].

## ACKNOWLEDGEMENTS

This study was supported by the Serbian Ministry of Science, Technological Development and Innovation from the grant 451-03-34/2026-03/200108.

## REFERENCES

[1] M. Jelali and A. Kroll, "Hydraulic servo-systems: Modelling, identification and control", Springer, https://doi.org/10.1007/978-1-4471-0099-7, (2003).

[2] N. Nedic, V. Stojanovic, and V. Djordjevic, "Optimal control of hydraulically driven parallel robot platform based on firefly algorithm", Nonlinear Dynamics, Vol. 82(3), pp. 1457–1473, https://doi.org/10.1007/s11071-015-2252-5, (2015).

[3] V. Stojanovic, N. Nedic, D. Prsic, LJ. Dubonjic, V. Djordjevic, "Application of cuckoo search algorithm to constrained control problem of a parallel robot platform", International Journal of Advanced Manufacturing Technology, 87(9-12), pp. 2497–2507, https://doi.org/10.1007/s00170-016-8627-z, (2016).

[4] V. Stojanovic, D. Prsic, "Robust identification for fault detection in the presence of non-Gaussian noises: Application to hydraulic servo drives", Nonlinear Dynamics, Vol. 100(3), pp. 2299–2313, https://doi.org/10.1007/s11071-020-05616-4, (2020).

[5] F. L. Lewis and D. Liu, "Reinforcement learning and approximate dynamic programming for feedback control", Wiley-IEEE Press, https://doi.org/10.1002/9781118453988, (2013).

[6] K. G. Vamvoudakis and F. L. Lewis, "Online actor-critic algorithm to solve the continuous-time infinite horizon optimal control problem", Automatica, Vol. 46(5), pp. 878–888, https://doi.org/10.1016/j.automatica.2010.02.018, (2010).

[7] T. Bian and Z.-P. Jiang, "Value iteration and adaptive dynamic programming for data-driven adaptive optimal control design", Automatica, Vol. 71, pp. 348–360, https://doi.org/10.1016/j.automatica.2016.05.003, (2016).

[8] F. L. Lewis and K. G. Vamvoudakis, “Reinforcement learning for partially observable dynamic processes: Adaptive dynamic programming using measured output data”, IEEE Transactions on Systems, Man, and Cybernetics, Part B (Cybernetics), Vol. 41(1), pp. 14–25, https://doi.org/10.1109/TSMCB.2010.2043839, (2010).

[9] F. Zhao, Z.-P. Jiang, T. Liu, “Event-triggered adaptive optimal control using output feedback: An adaptive dynamic programming approach,” in Proceedings of 38th Chinese Control Conference (CCC), July 27-30, (2019), pp. 1979-1984. https://doi.org/10.23919/ChiCC.2019.8866079.

[10] V. Djordjevic, H. Tao, X. Song, S. He, W. Gao, and V. Stojanovic, “Data-driven control of hydraulic servo actuator: An event-triggered adaptive dynamic programming approach,” Mathematical Biosciences and Engineering, Vol. 20(5), pp. 8561–8582, https://doi.org/10.3934/mbe.2023376, (2023).

[11] F. Zhao, W. Gao, T. Liu, and Z.-P. Jiang, “Adaptive optimal output regulation of linear discrete-time systems based on event-triggered output-feedback,” Automatica, Vol. 137, p. 110103, https://doi.org/10.1016/j.automatica.2021.110103, (2022).

[12] F. Zhao, W. Gao, T. Liu, and Z.-P. Jiang, “Event-triggered robust adaptive dynamic programming with output feedback for large-scale systems,” IEEE Transactions on Control of Network Systems, Vol. 10(1), pp. 63–74, https://doi.org/10.1109/TCNS.2022.3186623, (2023).

[13] P. Zhao, Z. Bao, X. Liu, J. Zhang, and K. Cai, “Event-triggered trajectory tracking control for quadrotor UAVs subject to external disturbances,” International Journal of Robust and Nonlinear Control, Vol. 35(11), pp. 4669-4685, https://doi.org/10.1002/rnc.7933, (2025).